Polytypic transformations in SiC : diuse X-ray scattering and Monte Carlo simulations

Alexandre Boulle, D. Dompoint, I. Galben-Sandulache, D. Chaussende

Polytypic transformations in SiC : diffuse X-ray scattering and Monte Carlo simulations

A. Boulle and D. Dompoint
Science des Procédés Céramiques et de Traitements de Surface (SPCTS)
CNRS UMR 7315, Centre Européen de la Céramique
12,rue Atlantis 87068 LIMOGES, France

I. Galben-Sandulache and D. Chaussende
Laboratoire des Matériaux et du Génie Physique (LMGP)
CNRS UMR 5628, Grenoble INP, Minatec,
3 parvis Louis Néel, BP 257,
38016 Grenoble Cedex 01, France
(Dated: 15 janvier 2015)

Solid state phase transitions in SiC are investigated using diffuse X-ray scattering and Monte Carlo simulations. As an example, the 3C-6H transformation is investigated in details. The transformation is modeled with a statistical algorithm based on the concept of double cross-slipping and subsequent dissociation of basal plane dislocations. The corresponding diffuse X-ray scattering curves are calculated and quantitatively compared with experimental data obtained from 3C-SiC crystals annealed at high temperatures (1700-2100°C). From the simulations, it is demonstrated that the transformation implies the multiplication and ordering of double and triple stacking faults (SFs). The transformation level and root-mean-squared strains associated with the dislocations could be determined from the simulations. The defect structure formed during the transition can be rationalized by considering the relative energies of the SFs. Using an axial next-nearest neighbor Ising interaction model we show that single SFs are not energetically favored, whereas the simultaneous occurrence of double and triple SFs implies their relative energy difference to remain below a critical value ($\sim$ 8-9%).

PACS numbers: 61.72.Dd, 61.72.Nn, 61.50.Ks, 81.05.Hd

I. INTRODUCTION

Silicon carbide (SiC) is a very promising material for semiconductor applications because of its superior electronic properties, high thermal and chemical stabilities, high-power and high-frequency capabilities, and high tolerance to radiation damage.[1] SiC is especially envisioned for electronic devices operating in harsh environments, *e.g.* in the aerospace or automotive industry. In recent years, SiC single crystals are also broadly used to produce large area graphene layers via thermal desorption of Si at high temperatures.[2–5] One of the most fascinating properties of SiC is its pronounced polytypism, *i.e.* the existence of several (more than 200) crystalline forms of SiC which only differ in the way in which C-Si bilayers are stacked in the primitive unit cell.[6] The simplest polytypes of SiC have a zinc-blende and wurtzite structure, where the former (noted 3C in the Ramsdell notation) is characterized by a pure cubic ABC stacking of the C-Si double layers, and the latter (2H) is characterized by a pure hexagonal ABA stacking of the C-Si double layers. Between these two extremes, an infinite number of stacking combinations are theoretically possible, giving rise to different polytypes with either hexagonal or rhombohedral symmetry. The most common polytypes are 4H, 6H and 15R, which respectively contain 4, 6 and 15 stacked bilayers in the primitive unit-cell.

Since its discovery one century ago,[7] the phenomenon of polytypism in SiC remains a topic of active research.[8–10] In particular it is still not settled whether the occurrence of a large number of polytypes, especially long-period polytypes, stems from kinetic reasons (*i.e.* spiral growth around screw dislocations with large Burgers vector) or thermodynamic reasons (*i.e.* the phase formed has the lowest energy).[6,11] Similarly, the transformation between different polytypes is only poorly understood. Although it is broadly admitted that these polytypic transitions take place by the spatial ordering of stacking faults (SFs), the mechanisms governing their multiplication, expansion and ordering remain unclear.

In this paper, with the example of the 3C-6H transition, we investigate in details the mechanics of polytypic transformations in SiC using diffuse X-ray scattering (DXS) and Monte Carlo simulations. Particular attention will be paid to the statistical properties of the defect structure, the type of SF formed and the structure and energies of the disordered polytypes. From a technological point of view, the 3C-6H transition is important since it is believed to take place during the high-temperature (>1900°C) vapor-phase growth of 3C-SiC single crystals.[12] As a result, the grown crystals are of poor crystalline quality with high densities of SFs, which obliterates their use in electronic devices. The 3C-6H (and the reverse 6H-3C) transition has been studied both theoretically[9] and experimentally using Raman scattering,[13,14] transmission electronic microscopy (TEM)[15] and X-ray diffraction.[16] However, these stu-

dies reached contradictory conclusions regarding the possible transformation mechanism. In a recent study[17,18] we demonstrated that the 3C-6H transition involves the glide of partial dislocations according to a mechanism first proposed by Pirouz and Yang,[15] and we determined the transformation kinetics. In the present paper we present a detailed study of the transformation mechanism taking place during the 3C-6H transition. On the basis of the dislocation-based mechanism mentioned earlier[15], we build a statistical algorithm that allows investigate all possible transformation paths. The corresponding DXS curves are generated using a Monte Carlo approach and compared with experimental data. The energies of the polytypes undergoing the transformation are calculated using an axial next-nearest neighbor Ising interaction model and it is shown that the defect structure formed during the transformation can be rationalized by considering the relative energy difference between the different type of SFs in SiC.

II. EXPERIMENTAL

We used 10×10 mm^2, 250 μm-thick, commercially available (001)-oriented 3C-SiC single crystals (HAST Corporation) grown by chemical vapor deposition on "undulant" (001) Si wafers.[19] In order to promote the structural phase transition, the crystal have been annealed at high temperature (1700, 1800, 1900 and 2100°C) during 5 h. The annealing experiments are conducted under 60 kPa of argon. The surface of the sample is slightly graphitized upon annealing. Before further experiments, the graphite layer is removed using a 500°C KOH melt.

DXS experiments have been conducted on a home-made high-resolution diffractometer mounted on high power (18 kW) X-ray source and coupled with a four reflections Ge(220) monochromator, which yields a parallel (divergence $\Delta\theta = 12$ arcsec) and monochromatic (wavelength spread $\Delta\lambda/\lambda = 1.4\times10^{-4}$) beam of CuK$\alpha_1$ radiation. The X-ray beam is 100 μm thick and 10 mm wide, the samples are mounted horizontally on a five movements sample holder and the diffracted X-rays are detected with a curved position sensitive detector.[20]

In zinc-blende structures, the SFs lie in the {111} planes which give rise to narrow diffuse streaks parallel to the different <111> directions in reciprocal space. In order to characterize the SF structure it is necessary to record the intensity along this streaks. Since the normal to the surface is [001], the different <110> direction have to be successively set parallel to the detection plane (the plane defined by the incidence and scattered waves). Moreover, since only those reflections for which $h+k+l \neq 3N$ (where N is an integer) are affected by the SFs,[21] we shall focus on reflections located along the $[hhh+2]$ row. This row makes an angle of 54.74°with the surface normal and it was scanned wide enough to include the 002 and 113 reflections.

The undulant (001) Si substrates exhibit trenches running parallel to the $[1\bar{1}0]$ direction resulting in the annihilation of the SFs in the direction perpendicular to the trenches during growth.[19] The $[1\bar{1}0]$ direction hence corresponds to the high SF density direction and it turns out that the 3C-6H transition actually mainly takes place along the $[1\bar{1}1]$ and $[\bar{1}11]$ directions. Conversely, only weak diffuse scattering was observed in the 90°equivalent orientation, indicating that the transformation does not significantly occur along [111] and $[\bar{1}\bar{1}1]$.[18] All results presented below hence correspond to the orientation where the transformation is observed.

For the inspection of phase transitions in SiC it is convenient to use a common reference frame for all polytypes. We shall therefore describe 3C-SiC using a hexagonal unit-cell containing three C-Si bilayers stacked along $[001]_h$, where the hexagonal $[001]_h$ direction is parallel to the [111] direction of the cubic unit cell. The corresponding lattice vectors $\mathbf{a}_h$, $\mathbf{b}_h$, $\mathbf{c}_h$ are obtained from the cubic lattice vectors $\mathbf{a}$, $\mathbf{b}$, $\mathbf{c}$ according to[21] $\mathbf{a}_h = 1/2(\mathbf{b}-\mathbf{a})$, $\mathbf{b}_h = 1/2(\mathbf{c}-\mathbf{b})$ and $\mathbf{c}_h = \mathbf{a}+\mathbf{b}+\mathbf{c}$. With this transformation, the cubic $[hhh+2]$ direction becomes $[10L]_h$, in the hexagonal unit-cell.

III. STRUCTURE MODEL OF THE TRANSFORMATION

A. The 3C-6H transformation mechanism

Stacking faults can be created by the motion of partial dislocations, which result from the dissociation of perfect basal plane dislocations. For instance a screw dislocation with Burgers vector $[100]_h$ dissociates into two 30°partial (Shockley) dislocations according to[22] :

$$[100]_h \rightarrow 1/3[210]_h + 1/3[1\bar{1}0]_h \qquad (1)$$

Using the standard ABC notation, the first partial shifts all planes above the dislocation from position A to B (B to C and C to A), thereby creating a intrinsic SF (noted 1SF in Fig. 1(a)), and the stacking sequence in changed from (ABC)(ABC)(ABC)... to (ABC)(A|CA)(BCA)... (where | indicates the slip plane). The second partial dislocation shifts the planes back from B to A (C to B and A to C). First principle calculations revealed that SFs in 3C-SiC actually have a negative formation energy[23–26] so that both partials repel each other, hence creating an extended SF region between them. Since the two partial dislocations have different core structures (a pure Si and a pure C core) they also exhibit different mobilities, the Si-core dislocation being the most mobile.[27,28] This asymmetry in the mobilities is the basis of the transformation mechanism suggested by Pirouz and Yang[15] : the mobile dislocation extends laterally and forms a faulted loop according to a Frank-Read mechanism.[29] However, in contrast with a classical Frank-Read source, a second operation of the loop on the same plane is forbidden as it would generate an AA-type stacking. The overlap of the strain fields of

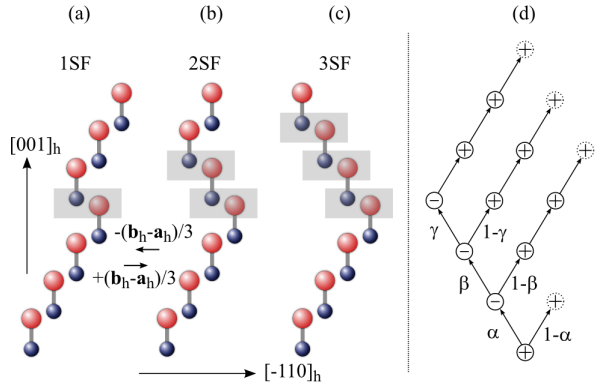

FIGURE 1. Schematic representation of the single (a), double (b) and triple (c) stacking fault in 3C-SiC ; The blue and red spheres represent C and Si, respectively. The gray area highlights the fault plane. (d) Statistical algorithm for the polytypic transition. α, β and γ denote the probabilities to fault three successive planes, respectively. Each fault is followed by a region of three bilayers without faults. At the end of each branch (dotted circles), the process is repeated.

both partials then causes the dislocation to reach the neighboring $(001)_h$ plane by double cross-slipping, where a new faulted loop can be created thereby creating a double (extrinsic) SF (noted 2SF in Fig. 1(b)) and changing the stacking sequence to (ABC)(AC|B)(CAB)... . If this process is repeated once, a triple SF (3SF) is formed (Fig. 1(c)) and the corresponding stacking sequence is (ABC)(ACB|)(ABC)..., where the sequence contained in the two first parenthesis correspond to the stacking sequence of the 6H polytype.

We casted this double cross-slipping concept into the statistical algorithm described below, Fig. 1(d). For convenience we make use of the binary Hägg notation which turns out to be more tractable than the classical ABC notation, especially when dealing with SFs. In the Hägg notation, the layers are denoted according to their relative orientations : the cyclic sequences AB, BC and CA (which correspond to a $+(\mathbf{b}_h - \mathbf{a}_h)/3$ translation, Fig. 1) are denoted with a + sign, whereas the anti-cyclic sequences AC, BA, CB (which correspond to a $-(\mathbf{b}_h - \mathbf{a}_h)/3$ translation, Fig. 1) are denoted with a − sign. With this notation the glide of the first partial of Eq. (1) changes the sign of the bilayer above the glide plane from a + to a − sign and the stacking sequences in the 3C and 6H unit-cells are noted $(+++)$ and $(+++--)$, respectively. Starting with a screw dislocation pinned in the basal plane, we define three probabilities α, β, γ, which correspond to the probability for the dislocation to double cross-slip and form a faulted loop (hence, changing a + into − sign) in three successive planes, Fig. 1(d). Using this (α, β, γ) triplet, the single, double and triple SFs are noted (1,0,0), (1,1,0) and (1,1,1), respectively. Each type of SF is followed by a region of, a least, three bilayers where no SF occurs, which is compulsory in order to form the 6H sequence, $(+++)(---)(+++)$..., starting from the perfect 3C sequence $(+++)(+++)(+++)$... . According to Pirouz and Yang[15] this region where the Frank-Read source stops operating is due to the back-stress of the generated loops on the initial screw dislocation. Additionally we shall assume that the values taken by the different probabilities are either equal to one, or equal to each other. In the former case this implies, for instance, that once a SF is formed on a given glide plane, it is energetically favorable for the dislocation to fault the neighboring plane so as to form a double SF. The latter case is justified by the fact that the energy barrier for double cross-slipping and SF formation is the same whatever the glide plane considered.[9] The different faulting probabilities will therefore be represented by a single probability, τ, which corresponds to the transformation level. Inspection of Fig 1(d) reveals that the transformation can take place via four different paths :

(i) $\alpha = \tau \geq 0$, $\beta = \gamma = 1$. The transformation involves only triple SFs ; *i.e.* once a SF is formed on the first glide plane ($\alpha \neq 0$), the dislocation systematically faults the two adjacent planes.

(ii) $\alpha = \beta = \tau \geq 0$, $\gamma = 1$. The transformation involves single and triple SFs.

(iii) $\alpha = \gamma = \tau \geq 0$, $\beta = 1$. The transformation involves double and triple SFs.

(iv) $\alpha = \beta = \gamma = \tau \geq 0$. All type of SFs are possible.

The process depicted in Fig. 1(d) is repeated sequentially so that, in principle, a single dislocation is sufficient to completely transform a 3C-SiC crystal. In practice however the movement of the dislocation is hindered either by the presence of structural defects or dislocations gliding in another glide plane (*i.e.* another equivalent {111} plane of the cubic structure) so that a complete conversion into the 6H phase is never achieved[18] : the partially transformed crystals contain bands (corresponding to slip bands) of disordered SiC co-existing with a pure 3C matrix.

The previous algorithm has been used to generate faulted crystals with increasing SF density, according to each of the four possible transformation paths. In each case we computed the DXS intensity distribution according to the Monte Carlo scheme described below. Monte Carlo methods have been used in earlier works to investigate the effects of SFs[30–33] or polytypic transitions[34,35] on the diffracted X-ray intensities. However in these studies (with the noticeable exception of Ref. 33 which is focused on the study of random SFs) the calculations were not used to quantitatively analyze experimental data. We show below that the development of a suitable theoretical description of DXS including both the effects of different configurations of SFs and all experimental factors affecting the diffracted intensity allows to obtain a complete description of the statistical properties of the SF distribution at all stages of the 3C-6H transformation.

B. Diffuse X-ray scattering

The X-ray amplitude scattered from a SiC single crystal results from the coherent sum of the amplitudes, $f_{\rm SiC}$, scattered from the individual SiC units (schematically represented in Fig. 1) :

$$E(\mathbf{Q}) = A f_{\rm SiC} \sum_n e^{i\mathbf{Q}\mathbf{r}_n} \tag{2}$$

and

$$f_{\rm SiC} = f_{\rm C} + f_{\rm Si} e^{i\mathbf{Q}\mathbf{z}} \tag{3}$$

where $f_{\rm C,Si}$ are the atomic scattering factors of C and Si, and $\mathbf{z} = \mathbf{c}_h/4$ is the relative Si-C distance in a SiC unit. $\mathbf{Q} = \mathbf{K}_d - \mathbf{K}_i$ is the scattering vector, the difference between the wave vectors of the diffracted and incident beams. A is a function of the scattering angle containing the amplitude of the primary beam, the polarisation factor, etc.[21] We denoted $\mathbf{r}_n$ the position vector of the n^{th} SiC unit in the crystal. The hexagonal unit-cell of the 3C polytype contains three SiC units, so that $\mathbf{r}_n$ can be written

$$\mathbf{r}_n = n_1\mathbf{a}_h + n_2\mathbf{b}_h + n_3\frac{\mathbf{c}_h}{3} + \nu(n_3)\boldsymbol{\delta} \tag{4}$$

where $\boldsymbol{\delta} = (\mathbf{b}_h - \mathbf{a}_h)/3$ is the lateral translation between two SiC units. The function $\nu(n_3)$ determines the lateral translation of the n^{th} unit with respect to the first one. It is hence solely dependent on the nature of the polytype and on the presence of SFs and can be written :

$$\nu(n_3) = \sum_{j \le n_3} \sigma_j \tag{5}$$

where $\sigma_j = \pm 1$ is the pseudo-spin of the Hägg notation. It can be noticed that since $3 \times \boldsymbol{\delta}$ is an integer linear combination of the lattice parameters, $\nu(n_3)$ can be considered *modulo* 3, *i.e.* it simply corresponds to a sequence of 0,1 and 2. With these definitions, the scattered amplitude can be written :

$$E(\mathbf{Q}) = \Psi(\mathbf{Q}) \sum_{n_3=1}^{N_3} e^{in_3\mathbf{Q}\mathbf{c}_h/3} e^{i\nu(n_3)\mathbf{Q}\boldsymbol{\delta}} \tag{6}$$

and

$$\Psi(\mathbf{Q}) = A f_{\rm SiC} \sum_{n_1=1}^{N_1} \sum_{n_2=1}^{N_2} e^{i\mathbf{Q}(n_1\mathbf{a}_h + n_2\mathbf{b}_h)} \tag{7}$$

where N_3 is the number of coherently irradiated C-Si bilayers, and $N_{1,2}$ correspond to the lateral extension of the bilayers. Eq. (6) shows that the function $\nu(n_3)$ determines the relative phase shift between the waves scattered from successive bilayers. Previous experiments on faulted 3C-SiC[17] revealed that the reciprocal space intensity distribution has the shape of a narrow streak perpendicular to the bilayer plane. This is due to the fact that the lateral extension of the C-Si bilayers is close to or larger than the coherence length of the incoming beam. In the following we shall therefore consider that $N_{1,2} \to \infty$ so that the double sum in Eq. (7) can be replaced by a delta function, *i.e.* we only consider the intensity distribution in the direction normal to the C-Si bilayers.

A SiC polytype containing SFs is characterized by a particular function $\nu(n_3)$ from which the scattered amplitude can be straightforwardly computed using Eqs. (6-7). However, in an actual experiment the irradiated volume is much larger than the coherence volume of the incident beam, so that the recorded intensity is given by the incoherent sum of the intensities emanating from different coherently irradiated regions, each being characterized by a distinct microscopic SF distribution. The corresponding intensity is written $I(Q) =< |E(\mathbf{Q})|^2 >$, where the average $< ... >$ is performed over the different SF configurations. This average can be performed using a Monte Carlo method :

- using the statistical algorithm described in Fig. 1(d), we generate M faulted crystals (each containing N_3 C-Si bilayers)
- the corresponding scattered amplitudes $E_m(\mathbf{Q})$ and intensities $I_m(\mathbf{Q}) = |E_m(\mathbf{Q})|^2$ are computed using Eqs. (5-7).
- the averaged diffuse scattering intensity is finally obtained from :

$$I_d(\mathbf{Q}) = \frac{1}{M}\sum_{m=1}^{M} I_m(\mathbf{Q}) \tag{8}$$

As outlined above, the multiplication of SFs results from the motion of partial dislocations. These defects are characterized by the presence of a strain field around the dislocation line[29] which distorts the crystal lattice; these distortions in turn affect the scattered intensity.[36] The description of the diffraction effects from dislocations is the topic of intensive research[37,38] which is clearly out of the scope of this paper. Moreover, since the partial dislocations are randomly distributed in the volume of the crystal, a rigorous treatment would require a complete three-dimensional evaluation of the scattered intensity which would significantly impair the computing time. Instead we make use of the following treatment, which turns out to be sufficient for the purpose of analyzing the SF structure in SiC. The strain fields associated to the dislocations give rise to randomly distributed strain in the bulk of the crystal : this effect can be approximated by assuming that each of the M crystals generated is characterized by different level of strain ε with a probability density function $p(\varepsilon)$. The probability density function $p(\varepsilon)$ is assumed to be a Gaussian distribution with average 0 and standard deviation σ_ε, which yields Gaussian peak profile shapes (which is generally observed in the case of high dislocation densities[38]). In the Monte Carlo procedure we generate random values of ε possessing a Gaussian distribution with well-established

pseudo-random numbers generators. The scattered intensity along the $[10L]_h$ row is finally written :

$$I_m(\mathbf{Q}) = \left| \Psi(L) \sum_{n_3=1}^{N_3} e^{2\pi i n_3 (L+\varepsilon)/3} e^{2\pi i \nu(n_3)(1+\varepsilon)/3} \right|^2 \quad (9)$$

and

$$\mathbf{Q}_{[10L]_h} = 2\pi(\mathbf{a}_h^* + L\mathbf{c}_h^*) \quad (10)$$

where $\mathbf{a}_h^*$ and $\mathbf{c}_h^*$ are the reciprocal lattice basis vectors. In addition to the amplitude scattered from a single SiC unit, f_{SiC}, and the intensity of the primary beam, the function $\Psi(L)^2$contains the polarisation factor and the irradiated sample volume, which are both explicit functions of L. Detailed expressions have been given elsewhere[20] and won't be detailed here. Simulations (not shown here) revealed that the inclusion of random strains gives rise to a peak broadening which scales linearly with L, *i.e.* the effect is more pronounced in the high-L region. Moreover, the shape of the broadened peaks depend on the nature of the probability density function $p(\varepsilon)$. Several possible $p(\varepsilon)$ have been tested (Gaussian, Lorentzian,...) and, whereas none allowed to perfectly fit the data, the Gaussian distribution turned out to provide a rather good agreement with the observed data as will be shown in the next section.

As outlined in the previous section, the partially transformed SiC crystals are actually constituted of bands of disordered SiC with SFs, coexisting with pure 3C. The total diffracted intensity is therefore written as the incoherent superposition of the diffuse scattering emanating from the disordered SiC ($I_d(L)$) and the coherent intensity emanating from the pure SiC regions ($I_{3C}(L)$) :

$$I_t(L) = xI_d(L) + (1 - x_t)I_{3C}(L) \quad (11)$$

where x is volume fraction of disordered SiC. The expression for $I_{3C}(L)$ can be calculated using Eq. (9) and, noting that for the 3C polytype $\nu(n_3)$ generates a sequence of the type 012012..., we obtain

$$I_{3C}(L) = \Psi(L)^2 \frac{\sin^2\left[(\pi/3)N_3(L+1)\right]}{\sin^2\left[(\pi/3)(L+1)\right]} \quad (12)$$

This function exhibits peaks at $L + 1 = 3N$(where N is an integer) and periodic fringes with spacing $3/N_3$. In an actual experiment such fringes are not observed. This stems from the fact that (i) the number of C-Si bilayers, N_3, is in general high ($\backsim$ 1000 or more) so that individual fringes can not be resolved and (ii), the size of the coherently illuminated domains is not a constant, *i.e.* N_3 varies from one coherent domain to another which smears out the fringe structure. The intensity diffracted from the 3C regions is obtained from the incoherent superposition of the intensities diffracted by different coherent domains with different sizes :

$$I_{3C}(L) = \Psi(L)^2 \int_{N_3-3\sigma_{N_3}}^{N_3+3\sigma_{N_3}} p(N_3) \times \frac{\sin^2\left[(\pi/3)N_3(L+1)\right]}{\sin^2\left[(\pi/3)(L+1)\right]} dN_3 \quad (13)$$

where $p(N_3)$ is the probability density function of N_3. The average value of N_3 is chosen so that the width of the calculated Bragg peaks matches the width observed experimentally. For $p(N_3)$ we have chosen a (truncated) Gaussian function with a standard deviation high enough to completely smear out the fringe structure, *i.e.* $\sigma_{N_3} = N_3/3$ (the integration limits in Eq. (13) allow to integrate 99.9% of the Gaussian distribution while excluding unphysical negative values of N_3). Since Eq. (13) is independent of the SF distribution, it is calculated once outside the Monte Carlo loop which allows keeping the computing time as low as possible.

Finally, the intensity distribution recorded in an actual measurement is given by the convolution of $I_t(L)$ scattered from the sample, Eq. (11), with the resolution function $R(L)$ of the diffractometer :

$$I(L) = \int R(L')I_t(L - L')dL' \quad (14)$$

The resolution of the diffractometer is very well described with a Gaussian function, the full-width at half maximum (FWHM) of which correspond to the inverse of the coherence length along the scanning direction. This FWHM can be evaluated by the measurement of a raw, high-quality, 3C-SiC single crystal. For such a crystal we obtain FWHM = 0.006, 0.01 for the (002) ($L = 2$) and (113) ($L = 5$) reflections, respectively.

IV. RESULTS AND DISCUSSION

A. Diffuse X-ray scattering

Using Eq. (8-14) we performed simulations for all four possible transformation paths, with increasing transformation level ($\tau = 0$, 1, 5, 10, 15,..., 85, 90, 95, 99, 100%). The number of defect configurations used to evaluate the Monte Carlo average, Eq. (8), was fixed to 1000, which allows the standard deviation of the average intensity[33,38] to be lower than 3%. In all calculations the volume fraction of disordered SiC was set to 100%, Eq. (11), in order to focus on the evolution of the diffuse scattering. Additionally, for these simulations we did not include the effect of dislocation-induced strain ($\varepsilon = 0$ in Eq. (9)), as it is not directly related to the transformation mechanism and it only gives rise to a broadening of the peaks in the high-L region. The results are displayed in Figs. (2-5) for mechanisms (i-iv), respectively.

The main result that emerges from these simulations is that the different transformation paths give rise to very

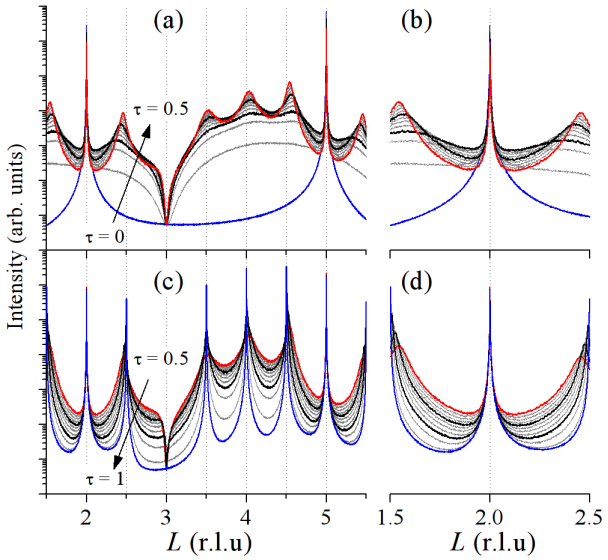

FIGURE 2. Evolution of the diffuse X-ray scattering for the mechanism (i), implying only triple SFs. (a) Evolution for τ = 0, 1, 5, 10, 15,... , 45, 50%. For a better reading of the figure, the curves corresponding to 0 (blue), 10 (black), 30 (black) and 50% (red) are represented with thick lines. (b) Zoom on the 1.5-2.5 region. (c) Evolution for τ = 50, 55, 60,... 90, 95, 99, 100%. The curves corresponding to 50 (red), 70 (black), 90 (black) and 100% (blue) are represented with thick lines. (d) Zoom on the 1.5-2.5 region.

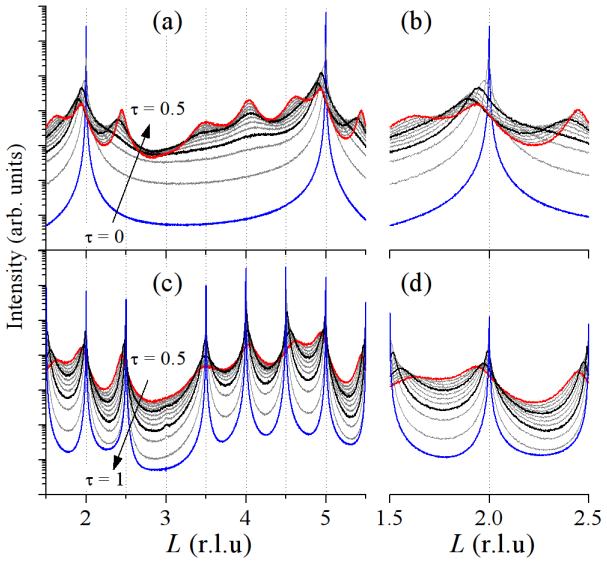

FIGURE 3. Same as in Fig. 2 for mechanism (ii) implying triple and single SFs.

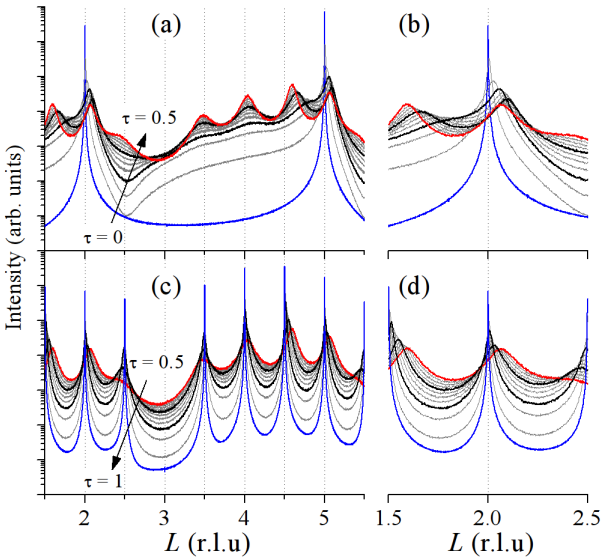

FIGURE 4. Same as in Fig. 2 for mechanism (iii) implying triple and double SFs.

distinct evolutions of the scattered intensity distribution. Common to all four paths is, in the very early stages of the transformation, the emergence of a broad DXS signal located between the Bragg peaks of the 3C phase (at $L = 2$ and $L = 5$). This DXS is directly due to the appearance of isolated SFs of different types. The total intensity of the diffuse scattering progressively increases up to $\tau \backsim 50\%$ indicating an increase of the SF density. For a transformation level of $\backsim 10\%$ broad peaks, located at $L \approx 2.5, 3.5, 4$ and 4.5, appear in the DXS. These pseudo-peaks correspond to the Bragg peaks of the upcoming 6H phase, although their position may initially significantly differ from their theoretical positions. For increasing τ, the pseudo-peaks are becoming sharper and progressively shift towards their theoretical location. For transformation levels larger than $\backsim 50\%$ the DXS located between the pseudo-peaks decreases while the SF structure progressively forms the final 6H structure.

For mechanisms (ii-iv), Figs. (3-5), the Bragg peaks of the 3C phase are broadened and shifted upon increasing transformation level. This indicates that the long range order of the 3C phase is lost, and the coherent Bragg peaks are replaced with (broadened and shifted) diffuse scattering peaks which, contrarily to coherent peaks, are sensitive to the defect structure of the crystal.[36] On the contrary, for mechanism (i), Fig. 2, the coherent peak remains throughout the transition and only its intensity is affected (although this is hardly visible in Fig. 2). Since mechanism (i) only involves triple SFs, in terms of the $\nu(n_3)$ function, a perfect 3C sequence is written 012[012]012, and a faulted 3C sequence, 012[102]012 (the square brackets indicate the faulted region) : the phase relationships between the planes outside the defect are unchanged between the 3C and the faulted 3C phase so that long range order is preserved and only the intensity of the Bragg peak is lowered. It can be straightforwardly noticed that this situation does not occur for single (sequence 012[1]201) and double (sequence 012[10]120) SFs and long range order is hence destroyed for mechanisms

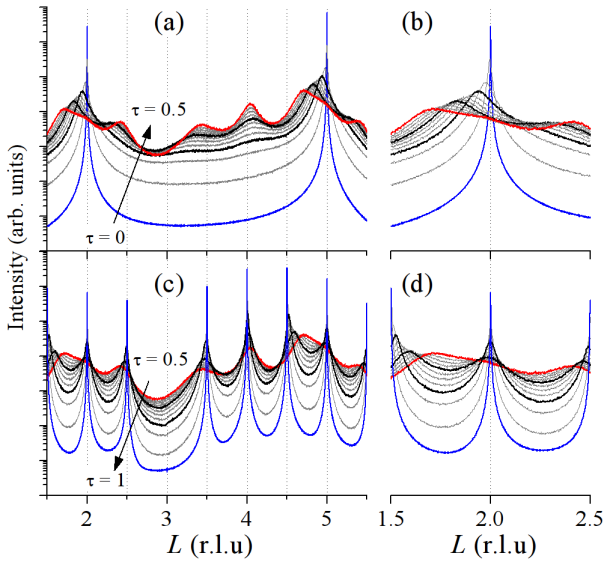

FIGURE 5. Same as in Fig. 2 for mechanism (iv) implying triple, double and single SFs.

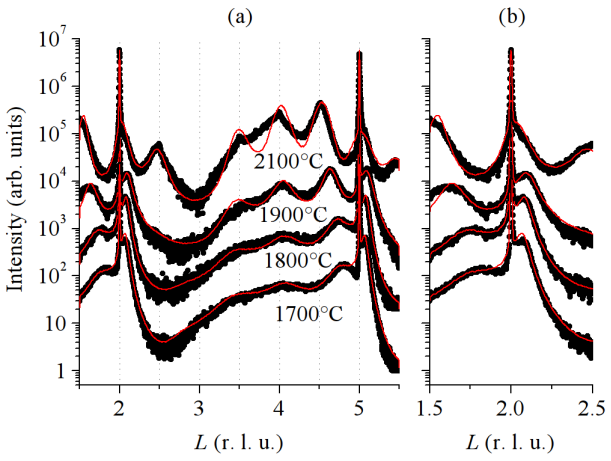

FIGURE 6. (a) Experimental DXS curves recorded along the $[10L]_h$ row (black circles) and Monte Carlo simulations (red lines) corresponding to 3C-SiC crystals annealed at increasing temperatures. (b) Zoom on the 1.5-2.5 region. For clarity, the curves are shifted vertically.

implying these defects.

The mechanisms implying single SFs, (ii) and (iv) (Fig. 3 and 5), are characterized, in the very early stages of the transformation by a symmetric DXS distribution around the Bragg peaks. This is a well known result for the diffuse scattering from isolated and independent (*i.e.* without spatial correlations) single SFs.[39] This indicates that in the early stages of the transition mainly single SFs are formed. On the contrary, when double (iii) and triple (i) SFs are formed the DXS intensity distribution is asymmetric, Fig. 2 and 4. For mechanism (i), Fig. 2, a deep minimum is observed at $L = 3$. This is due to the fact that crystals undergoing this mechanism are solely built of sequences of type 012012 (3C) and 012102 (faulted 3C). For both sequences, the sum in Eq. (9) vanishes for $L = 3$ (the same argument explains the absence of a Bragg peak at L=3 in the 6H phase), which is equivalent to the visibility condition mentioned in sec. II. On the contrary, crystals undergoing mechanism (iii) contain triple and double SFs. They are therefore built with the following sequences : 012012, 012102 (3SF) and 01210 (2SF), where the latter does not give rise to a vanishing sum in Eq. (9) ; hence no minimum is observed. The same argument can be used to explain the lack of a sharp minimum for mechanisms (ii) and (iv).

The qualitative comparison of the features of the calculated DXS curves with experimental data, Fig. 6, allows to conclude unambiguously that the transformation of annealed 3C-SiC crystals implies double and triple SFs, as described by mechanism (iii). The simulated curves for mechanism (iii) are also plotted in Fig. 6. The observed and calculated curves agree very well : for the first three temperatures (1700, 1800 and 1900°C) the fit is close to perfect. From these fits we determined the transformation level, τ, the volume fraction of disordered SiC, x, and the root-mean-squared (rms) deviation of the strain σ_ε ; the values are reported in table I.

Increasing the annealing temperature results in an increase of the transformation level, *i.e.* new dislocations, and thereby new SFs, are formed by double cross-slipping. It should be mentioned that, using the values given in table I, the activation energy for double cross-slipping deduced from an Arrhenius plot (*i.e.* $\ln(\tau)$ *vs.* $1/T$) is 1.7(1) eV, in very close agreement with the (only available) theoretical value of 1.54 eV obtained by Käckell *et al.*[9] using density functional theory calculations. In Fig. 6, the increase of τ is responsible for the progressive structuration of the DXS intensity distribution. The transformation is initiated in different regions of the crystals and, because the motion of the dislocation is hindered by structural defects (see Sec. III), the transformation is confined into (slip) bands of finite extension with total volume fraction x. The transformation level determined above is therefore averaged over the different disordered regions. Nevertheless, upon increasing temperature, the volume fraction increases (though slower than τ) indicating that the partial dislocations progressively fault extended regions of the crystal. In Fig. 6 the increase of x appears as an increase of the total DXS intensity as compared to the coherent intensity emanating from the 3C regions. Together with the increase of the SF density, we also observe an increase of the rms strain which can be attributed to the strain fields associated to the partial dislocations. As outlined in the previous section, random strains yield a broadening of the intensity distribution that scales with L. For the two lowest temperatures, the transformation level is relatively low (14 and 16%) so that the strain fields produce negligible effects of the broad DXS signal. On the contrary, for the two

TABLE I. Values of the transformation level, volume fraction and root mean-squared strain obtained for 3C crystals annealed at increasing temperature.

Temperature (°C)	Transformation level τ (%)	Volume fraction x_t	r.m.s. strain (%)
1700	14	23	0
1800	16	40	0
1900	35	49	0.6
2100	70	60	1.5

TABLE II. Values of the coefficients J_i and K (expressed in meV / SiC pair) entering Eq. (15), according to different groups. E(nSF) are the energies (in meV) of the SFs containing n successive faulted planes. The relative energy difference between the 3SF and 2SF is expressed in %.

	Cheng et al. (1990)[40]	Park et al. (1994)[41]	Bernstein et al. (2005)[10]	Käckell et al. (1998)[23]	Cheng et al. (1988)[42]	Iwata et al. (2002)[43]	Limpijumnong et al. (1998)[44]	Rutter et al. (1997)[45]	Karch et al. (1994)[46]
J_1 (meV/SiC)	2.33	2.0	2.588	1.18	5.33	1.91	3.562	3.45	4.80
J_2 (meV/SiC)	-3.49	-3.40	-3.25	-2.34	-3.42	-2.306	-2.550	-2.70	-2.93
J_3 (meV/SiC)	0.25	-0.20	-0.288	-0.32	-0.39	-0.396	-0.862	-0.45	-0.45
K (meV/SiC)	0	0	-0.0125	0	0.21	0	0.488	0	0
E(1SF) (meV)	-3.64	-6.40	-3.90	-5.92	7.76	-3.168	4.504	1.20	5.68
E(2SF)(meV)	-16.60	-20.80	-18.0	-16.56	-8.32	-13.976	-11.096	-11.40	-7.84
E(3SF) (meV)	-15.60	-21.60	-19.20	-17.84	-9.04	-15.560	-12.592	-13.20	-9.64
(E(3SF)-E(2SF))/E(2SF)(%)	-6	3.85	6.67	7.73	8.65	11.33	13.48	15.79	22.96

highest temperatures, the transformation level is significantly higher (35 and 70%) which in turn gives rise to a significant strain-induced broadening. For the highest annealing temperature, it can be observed that the agreement between the experimental data and the simulation is less satisfactory, especially in the $L = 3.5$ - 4.5 region. This discrepancy is likely due to an oversimplification of the strain-induced effects, *i.e.* the probability density function of the strain is probably not easily described by a predefined (Gaussian, Lorentzian,...) function. A rigorous treatment would imply to take into account the displacement field associated to each partial dislocation and to calculate the scattered intensity distribution in the three dimensions[37,38]. As discussed in Sec. III this is out of the scope of this paper, and this would probably not drastically change the conclusions regarding the polytypic transformation since, in all cases, the simulations in the low L region (Fig. 6b) are close to perfect.

B. Polytype and stacking fault energies

The simulation of the DXS curves revealed that the 3C-6H transition implies the multiplication and ordering of double and triple SFs, as described by the statistical algorithm in Fig. 1(d). This behavior can be clarified by the inspection of the polytype energies during the transition. The computation of the ground-state energies of different SiC polytypes, with or without SFs, has attracted a lot of interest in the two past decades[10,23,40–46] and therefore a large amount of theoretical data is available. Part of this interest is due to the fact that, in the framework of the axial next-nearest-neighbor Ising (ANNNI) interaction model, SiC is close to a multiphase degeneracy point[47], *i.e.* the pronounced polytypism of SiC can be explained by energy considerations. In the ANNNI interaction model, including interactions up to the third neighbor, the energy per C-Si bilayer of a SiC polytype consisting of N_3 bilayers is written[42,44] :

$$E = E_0 - \frac{1}{N_3}\sum_i J_1\sigma_i\sigma_{i+1} + J_2\sigma_i\sigma_{i+2} + J_3\sigma_i\sigma_{i+3} + K\sigma_i\sigma_{i+1}\sigma_{i+2}\sigma_{i+3} \quad (15)$$

where E_0 is the energy of an isolated bilayer, the coefficients J_i represent the interlayer interaction energy and K is the four spin interaction energy. The latter parameter is very small and, hence, often neglected. The values of J_i and K (when available) are given in table II according to different authors[48]. The calculations performed by the different groups made use of different assumptions and different computational approaches, namely the density functional theory in the local-density approximation[23,40–43,45,46], in the generalized gradient approximation[44] or tight-binding calculations[10]. These studies therefore lead to different results for the absolute polytype energies. However, the energy ordering of the polytypes is mainly unchanged : the 4H (and occasionally 6H) is found the most stable polytype, 2H is the least stable and 3C has an intermediate energy. Also, most of these studies are based on the density functional theory and the calculations are therefore carried out at 0K. It

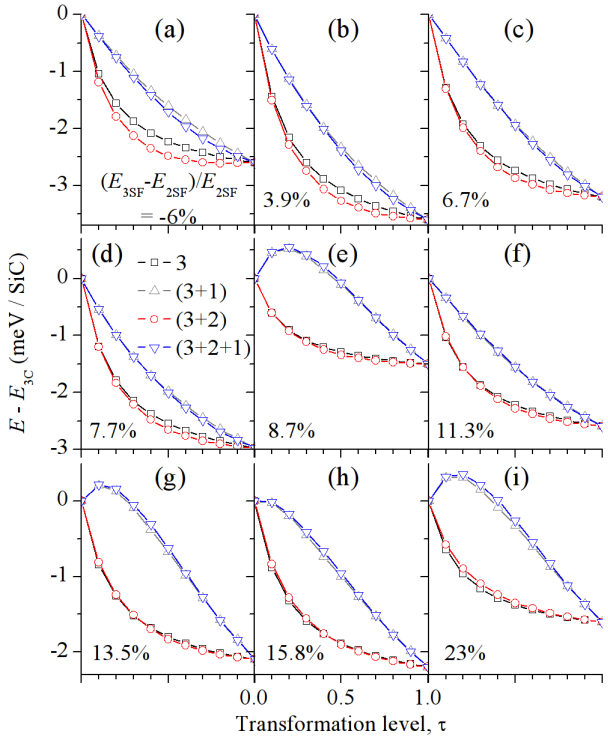

FIGURE 7. Evolution of the polytype energies for each mechanism, calculated with Eq. (15) using the coefficients given in table II. Squares : mechanism (i) (3SFs) ; triangles : mechanism (ii) (3SFs and 1SFs) ; circles : mechanism (iii) (3SFs and 2SFs) ; reversed triangles : mechanism (iv) (3SFs, 2SFs and 1SFs). Panels (a-i) are computed with the coefficients given in columns 2-10 of table II, respectively. The relative energy difference between the 3SF and the 2SF is given in each panel.

has however been demonstrated that the contribution of vibrational entropy only increases the free-energy differences between the polytypes without modifying their ordering.[8] The results obtained at 0K can hence safely be used to discuss polytypic transitions ; the differences obtained when using different J_i and K coefficients will be used to illustrate the role of SF energies.

The energy of the polytypes is calculated by applying Eq. (15) to the crystals generated to compute the DXS. For each polytype the energy is averaged over M different SF configurations and the resulting uncertainty on the average energy is better than 1%. The results are displayed in Fig. 7, where the energy difference relative to the 3C phase ($E - E_{3C}$) is plotted *vs.* the transformation level for all possible transformation paths and for the different values of J_i and K. In all cases, we observe that $E_{6H} < E_{3C}$, which constitutes the driving force for the transition. In panels (a-e) the decrease in energy is faster for mechanism (iii) (3SFs+2SFs). In panels (f-i), 3SFs are more favorable, at least in the first stages of the transition. The mechanisms implying single SFs (ii and iv) are characterized by a slower energy decrease, panels (a, b, c, d, f), or even by the appearance of an energy barrier, panels (e, g, h, i). These features make these latter mechanisms less likely to occur than mechanism (i) and (iii).

Let us now consider the SF energies ; they can be straightforwardly obtained from the energy difference between a faulted crystal and the regular 3C phase. Using Eq. (15) one obtains :

$$E(1SF) = 4(J_1 + J_2 + J_3 + 2K) \tag{16}$$

$$E(2SF) = 4(J_1 + 2J_2 + 2J_3 + K) \tag{17}$$

$$E(nSF; n \geq 3) = 4(J_1 + 2J_2 + 3J_3 + 2K) \tag{18}$$

The corresponding values are given in Table II. In all cases we observe that the energy of a single SF is significantly higher than the energy of a double and a triple SF. This implies that once a dislocation underwent double cross-slipping and faulted a given plane, it will be energetically favorable to double cross-slip one or two additional times in order to fault one or two additional planes, so that mechanisms implying single SFs are indeed not favored. The cases where E(1SF) > 0 give rise to the energy barrier observed in Fig. 7.

Surprisingly, excepted for one study[40], we obtain E(3SF) $<$ E(2SF). One would therefore expect the mechanism with 3SFs to prevail during the transition, contrarily to experimental evidence. This result is actually a consequence of the sequential nature of the double cross-slipping - based faulting mechanism, which produces different SF formation rates upon increasing transformation level. In the particular case of the 3C-6H transition, the SFs are separated by at least three regularly stacked C-Si bilayers. From the point of view of Eq. (15), which includes interaction up to the third neighbor, the different SFs formed during the transition are hence non-interacting defects. The energy per bilayer of a disordered polytype can therefore be equivalently written :

$$E = \frac{1}{N_3}[n_1 E(1SF) + n_2 E(2SF) + n_3 E(3SF)] \tag{19}$$

where $n_{1,2,3}$ are the number of SF of type 1, 2 and 3, respectively. The energy of the polytypes hence not only depends on the energy of the SF but also on the relative amount of SF formed. The values of n_i can be obtained by a direct counting in the crystals generated previously.

Fig. 8 represents the evolution of the relative fault fraction n_i/N_3 for all transformation paths. For mechanism (i), Fig. 8(a) shows that the formation of 3SFs is important from the early stages of the transformation. On the contrary, in mechanism (iii), Fig. 8(c), the formation of 3SFs is more progressive, whereas the formation

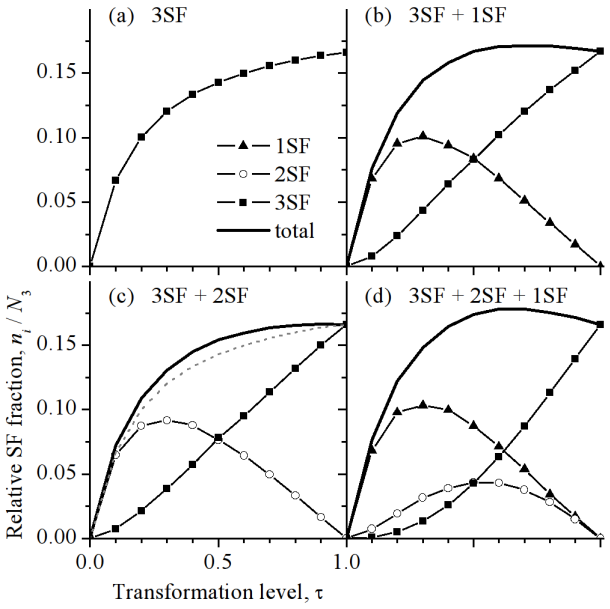

FIGURE 8. Evolution of the relative SF fraction for increasing transformation level. Panels (a-d) correspond to mechanisms (i-iv), respectively. Triangles : single SFs ; circles : double SFs ; squares : triple SFs; thick line : total SF fraction. In panel (c), the thin dotted line correspond to the total SF fraction of mechanism (i).

of 2SFs strongly increases up to $\tau = 30\%$ and then drops to 0. The key point is that the total defect concentration, $(n_2 + n_3)/N_3$, is higher for this mechanism (thick line in Fig. 8c) than the total defect concentration, n_3/N_3, occurring in mechanism (i) (dotted line in Fig. 8c). Hence, the mechanism implying 2SFs and 3SFs is energetically favorable, as long as the relative energy difference between 2SFs and 3SFs does not exceed a critical value (estimated to 8-9% from Fig. 7). Similarly, the strong increase of 1SFs occurring at the beginning of the transition in mechanisms (ii) and (iv), combined with the unfavorable SF energy, inhibits these transformation paths.

V. SUMMARY AND CONCLUSIONS

With the example of the 3C-6H transformation, we studied polytypic transitions in SiC using diffuse X-ray scattering and Monte Carlo simulations. A statistical algorithm, based on a double cross-slipping mechanism of faulting, has been developed to describe all possible transformation paths between the 3C and the 6H phases of SiC. Numerical crystals with increasing SF densities, corresponding to increasing transformation levels have been generated, and the corresponding diffuse X-ray scattering has been computed using a specifically developed theoretical description. The simulation of the experimental intensity distribution along the $[10L]_h$ row allowed to conclude that the transformation takes place by the multiplication and ordering of double and triple SFs. Moreover, the transformation level, the volume fraction of disordered material and the root-mean-squared strains could be obtained from these simulations, demonstrating the progress of the transformation and the increase of dislocation density upon increasing temperature. The numerical crystals have also been used to compute, using an ANNNI interaction model, the energy of the polytypes formed during the transformation as well as the SF energies. We showed that the transition is actually governed by the relative energy difference between double and triple SFs : the mechanism involving double and triple SFs is favored when this energy difference is smaller than 8-9%. Besides, the energy of single SFs prohibits any mechanism implying the presence of such defects.

ACKNOWLEDGMENTS

We thank the Region Limousin (France) for financial support. LMGP thank the MINTEX-French ANR program (Contract No. ANR-09-BLAN-0189-01) and the MANSiC-Marie Curie Research and Training Network (Contract No. MRTN-CT-2006-035735) for their financial support. All calculations have been performed using the Python programming language (www.python.org) combined with the SciPy scientific library (www.scipy.org). The corresponding developers and communities are gratefully acknowledged.

[1] A. Fissel, Phys. Rep. **379**, 149 (2003).
[2] C. Virojanadara, M. Syväjarvi, R. Yakimova, L. Johansson, A. Zakharov, and T. Balasubramanian, Phys. Rev. B **78**, 245403 (2008).
[3] A. Ouerghi, M. Marangolo, R. Belkhou, S. El Moussaoui, M. Silly, M. Eddrief, L. Largeau, M. Portail, B. Fain, and F. Sirotti, Phys. Rev. B **82**, 125445 (2010).
[4] F. Ming and A. Zangwill, Phys. Rev. B **84**, 115459 (2011).
[5] O. Pankratov, S. Hensel, P. Götzfried, and M. Bockstedte, Phys. Rev. B **86**, 155432 (2012).
[6] N. Jepps and T. Page, Prog. Cryst. Growth Charact. Mater. **7**, 259 (1983).
[7] H. Baumhauer, Z. Kristallogr. **50**, 33 (1912).

[8] A. Zywietz, K. Karch, and F. Bechstedt, Phys. Rev. B **54**, 1791 (1996).
[9] P. Käckell, J. Furthmüller, and F. Bechstedt, Phys. Rev. B **60**, 13261 (1999).
[10] N. Bernstein, H. Gotsis, D. Papaconstantopoulos, and M. Mehl, Phys. Rev. B **71**, 075203 (2005).
[11] G. Trigunayat, Sol. State Ionics **48**, 3 (1991).
[12] D. Chaussende, F. Mercier, A. Boulle, F. Conchon, M. Soueidan, G. Ferro, A. Mantzari, A. Andreadou, E. Polychroniadis, C. Balloud, S. Juillaguet, J. Camassel, and M. Pons, J. Cryst. Growth **310**, 976 (2008).
[13] W. Yoo and H. Matsunami, J. Appl. Phys. **70**, 7124 (1991).
[14] R. Püsche, M. Hundhausen, L. Ley, K. Semmelroth, F. Schmid, G. Pensl, and H. Nagasawa, J. Appl. Phys. **96**, 5569 (2004).
[15] P. Pirouz and J. W. Yang, Ultramicroscopy **51**, 189 (1993).
[16] V. Kabra, D. Pandey, and S. Lele, J. Mater. Sci. **21**, 1654 (1986).
[17] A. Boulle, J. Aube, I. Galben-Sandulache, and D. Chaussende, Appl. Phys. Lett. **94**, 201904 (2009).
[18] D. Dompoint, A. Boulle, I. Galben-Sandulache, D. Chaussende, L. Hoa, T. Ouisse, D. Eyidi, J. Demenet, M. Beaufort, and J. Rabier, J. Appl. Phys. **110**, 053508 (2011).
[19] H. Nagasawa, K. Yagi, T. Kawahara, and N. Hatta, Chem. Vap. Deposition **12**, 502 (2006).
[20] A. Boulle, D. Dompoint, I. Galben-Sandulache, and D. Chaussende, J. Appl. Crystallogr. **43**, 867 (2010).
[21] B. E. Warren, *X-ray Diffraction* (New-York : Addison-Wesley, 1969).
[22] In order to avoid multiple conversion from the cubic to hexagonal symmetry, we here don't make use of the four index hexagonal notation. With this notation the previous reaction would read $1/3[2\bar{1}\bar{1}0] \rightarrow 1/3[10\bar{1}0] + 1/3[1\bar{1}00]$.
[23] P. Käckell, J. Furthmüller, and F. Bechstedt, Phys. Rev. B **58**, 1326 (1998).
[24] U. Lindefelt, H. Iwata, S. Öberg, and P. Briddon, Phys. Rev. B **67**, 155204 (2003).
[25] H. Iwata, U. Lindefelt, S. Öberg, and P. Briddon, Phys. Rev. B **68**, 113202 (2003).
[26] T. Thomas, D. Pandey, and U. V. Waghmare, Phys. Rev. B **77**, 121203 (2008).
[27] X. Ning and P. Pirouz, J. Mater. Res. **11**, 884 (1996).
[28] S. Ha, M. Benamara, M. Skowronski, and H. Lendenmann, Appl. Phys. Lett. **83**, 4957 (2003).
[29] J. Hirth and J. Lothe, *Theory of dislocations*. (Wiley, New-York, 1982).
[30] R. Berliner and S. A. Werner, Phys. Rev. B **34**, 3586 (1986).
[31] B. I. Nikolin and A. Y. Babkevich, Acta Cryst. A **45**, 797 (1989).
[32] J. Gosk, Cryst. Res. Technol. **35**, 101 (2000).
[33] M. Barchuk, V. Holý, D. Kriegner, J. Stangl, S. Schwaiger, and F. Scholz, Phys. Rev. B **84**, 094113 (2011).
[34] V. K. Kabra and D. Pandey, Acta Cryst. A **51**, 329 (1995).
[35] S. P. Shrestha and D. Pandey, Proc. R. Soc. Lond. A **453**, 1311 (1997).
[36] M. A. Krivoglaz, *X-ray and neutron diffraction in nonideal crystals* (Springer, Berlin, 1996).
[37] V. Holý, T. Baumbach, D. Lübbert, L. Helfen, M. Ellyan, P. Mikulik, S. Keller, S. DenBaars, and J. Speck, Phys. Rev. B **77**, 094102 (2008).
[38] V. Kaganer and K. Sabelfeld, Phys. Rev. B **80**, 184105 (2009).
[39] M. Paterson, J. Appl. Phys. **23**, 805 (1952).
[40] C. Cheng, V. Heine, and R. J. Needs, J. Phys. : Condens. Matter **2**, 5115 (1990).
[41] C. H. Park, B.-H. Cheong, K.-H. Lee, and K. Chang, Phys. Rev. B **49**, 4485 (1994).
[42] C. Cheng, R. J. Needs, and V. Heine, J. Phys. C **21**, 1049 (1988).
[43] H. Iwata, U. Lindefeit, S. Öberg, and P. Briddon, Mater. Sci. Forum **389**, 439 (2002).
[44] S. Limpijumnong and W. Lambrecht, Phys. Rev. B **57**, 12017 (1998).
[45] M. Rutter and V. Heine, J. Phys. : Condens. Matter **9**, 8213 (1997).
[46] K. Karch, P. Pavone, W. Windl, O. Schütt, and D. Strauch, Phys. Rev. B **50**, 17054 (1994).
[47] J. Yeomans, Sol. State Phys. **41**, 151 (1988).
[48] When the coefficients are not directly available in the cited work, they have been computed by solving Eq. (15) for J_i, K and E_0 using the energies of five different polytypes, *e.g.* 2H, 3C, 4H, 6H and 15R.